The Zeeman tuning of the A $^6\Sigma^+$–X $^6\Sigma^+$ transition of chromium monohydride†

Jinhai Chen,[a] **Joost M. Bakker,**[bc] **Achim Peters,**[b] **Michael Stoll,**[c] **Gerard Meijer**[c] **and Timothy C. Steimle**[a]

The magnetic tuning of the low-rotational levels of the A $^6\Sigma^+$ (v = 1 and 0) states of chromium monohydride, ^{52}CrH, have been experimentally investigated using optical spectroscopy of the (0, 0) and (1, 0) bands of the A $^6\Sigma^+$–X $^6\Sigma^+$ transition. The tuning of the numerous low-rotational lines in the A $^6\Sigma^+$–X $^6\Sigma^+$ (0, 0) band can be accurately modeled using a single set of g-factors (g_S and g_ℓ) which are close to the expected values. In contrast, the g-factors for the A $^6\Sigma^+$ (v = 1) state required to model the magnetic tuning of low-rotational lines in the A $^6\Sigma^+$–X $^6\Sigma^+$ (1, 0) band are strongly dependent upon rotational and fine structure component and the determined effective values for g_S deviate significantly from 2.002. Interpretation of the quantum level variation of g_S is presented. The magnetic hyperfine structure of the (0, 0) and (1, 0) bands of the A $^6\Sigma^+$–X $^6\Sigma^+$ transition is analyzed to produce proton Fermi contact, b_F and dipolar, c, magnetic hyperfine parameters of 19(1) MHz and 34(5) MHz for the A $^6\Sigma^+$ (v = 0) state and 21(2) MHz and 30(7) MHz for the A $^6\Sigma^+$ (v = 1) state.

1. Introduction

Creating samples of cold and confined dipolar neutral molecules promises to allow for studies addressing several important physical questions, ranging from the possible variation of fundamental constants,[1] to the study of physics beyond the standard model by the measurement of a permanent electric dipole moment of the electron,[2] and the realization of a quantum computer.[3] As a consequence, several techniques have been developed over the last few years for cooling and trapping samples of cold molecules.[4] One such method is the buffer-gas cooling of molecules by injecting them at elevated temperature into a dense vapor of cold helium, typically at temperatures substantially below 1 K. The molecules will transfer their energy to the helium atoms through elastic collisions, and will finally thermalize with their cryogenic environment. If the buffer-gas cooling is done within a magnetic quadrupole trap and a molecule with a sufficiently high magnetic moment is chosen, the magnetic forces can confine molecules in quantum states for which the energy increases with the magnetic field, the so-called low-field seeking states. Buffer-gas cooling and magnetic trapping of calcium monohydride, CaH, was demonstrated in 1998 by Doyle and co-workers.[5] The magnetic properties of CrH are studied here as a necessary preliminary to our use of it in buffer-gas cooling and magnetic trapping experiments.

Not all molecules with a paramagnetic ground state are suitable for the combination of buffer-gas cooling and magnetic trapping. Since the buffer gas cooling method relies upon the use of elastic collisions between the molecule and the inert buffer gas, in order to cool the state, the occurrence of a significant number of inelastic, state-changing, collisions into the nearest low lying state renders the method ineffective. This is because the most probable accessible molecular state is a high field seeking one which will lead to molecules in this state being driven out of the trapping region. At present the role of helium in promoting inelastic collisions is poorly understood.

Based on the few theoretical investigations, which are limited to molecules in $^2\Sigma$ and $^3\Sigma$ ground states,[6,7] and the experimental data available for two $^2\Sigma$ molecules, CaH[5] and CaF,[8] we identified the high-spin ground state of chromium monohydride, CrH as a suitable candidate for buffer-gas cooling and magnetic trapping.[9] It is anticipated that the relatively large rotational spacing and small spin–spin and spin–rotation interaction in the X $^6\Sigma^+$ (v = 0) state is a signature of a favorable ratio of elastic to inelastic collisions with helium atoms. Furthermore, the large magnetic moment of the N = 0, X $^6\Sigma^+$ (v = 0) state of CrH enables one to create a deep trap, and this allows a large enough trapping time to be able to isolate the sample from its environment by cryopumping the helium away.

Understanding the energy levels and Zeeman tuning of the X $^6\Sigma^+$ (v = 0) state is crucial for buffer-gas cooling and magnetic trapping. Fortunately, the field-free energy levels and magnetic tuning of the low-rotational levels of the X $^6\Sigma^+$ (v = 0) state are known from laser magnetic resonance (LMR)[10] and mm-wave[11] pure rotational spectra. Modeling the field-free energies and magnetic tuning of the low-rotational levels (N = 0, 1 and 2) of the A $^6\Sigma^+$ (v = 0 and 1) state

^{a} *Department of Chemistry and Biochemistry, Arizona State University, Tempe, AZ 85287-1604, USA. E-mail: tsteimle@asu.edu*
^{b} *Humboldt Universität zu Berlin, Institut für Physik, Hausvogteiplatz 5-7, 10117 Berlin, Germany*
^{c} *Fritz-Haber-Institut der Max-Planck-Gesellschaft, Faradayweg 4-6, 14195 Berlin, Germany*
† Electronic supplementary information (ESI) available: Observed and calculated Zeeman shifts. See DOI: 10.1039/b614927h

is also vital to the development of buffer-gas cooling and magnetic trapping of CrH because the intense (0, 0) band at 866 nm and the (1, 0) band at 767 nm of the A $^6\Sigma^+$–X $^6\Sigma^+$ electronic transition are convenient for monitoring the spatial and temporal molecular concentrations of CrH in the trap. The (1, 0) band is of particular interest because it is at a convenient wavelength for excitation while the resulting off-resonant (1, 1) fluorescence near 874 nm can be selectively detected without interference from scattered laser light. Similar optical spectroscopic monitoring was performed in the buffer-gas cooling and trapping experiments for CaH.[5]

The field-free optical spectrum of a high-temperature sample of CrH has been thoroughly investigated at Doppler-limited resolution, motivated in part by its astrophysical importance.[12] The optical spectrum of a cold sample produced by supersonic expansion has been investigated using time-delayed resonant two-photon ionization spectroscopy[13] and moderate resolution laser induced fluorescence (LIF);[14] a review of the spectroscopy of CrH can be found in these references as well. The high-resolution spectrum of the A $^6\Sigma^+$–X $^6\Sigma^+$ electronic transition is complex because each rotational level of the A $^6\Sigma^+$ and X $^6\Sigma^+$ states is split into up to six ($= 2S + 1$) fine structure components due to spin–rotation and spin–spin interactions. The fine structure splitting, which is dominated by second-order spin–orbit effects, is large in the A $^6\Sigma^+$ state because of the high-density of electronic states, giving rise to six spectrally distinct intense P and R branches. Each of these branch features exhibits a small, proton, magnetic hyperfine splitting, heretofore not resolved. The most abundant (84%) ^{52}Cr isotope has no nuclear spin. There have been no previous sub-Doppler field-free or Zeeman optical studies of the A $^6\Sigma^+$–X $^6\Sigma^+$ electronic transition and thus no analysis of the magnetic tuning or proton magnetic hyperfine splitting of the optical lines.

Modeling A $^6\Sigma^+$–X $^6\Sigma^+$ spectra with an effective Hamiltonian has been difficult because of strong perturbation in the A $^6\Sigma^+$ state by, primarily, the a $^4\Sigma^+$ state. The a $^4\Sigma^+$ ($v = 0$) vibronic state has been experimentally determined[15] to lie only 367 cm^{-1} below the A $^6\Sigma^+$ ($v = 0$) state and causes local perturbations that maximize near $N \approx 9$ and $N \approx 21$ in the A $^6\Sigma^+$ ($v = 0$) vibronic state. The A $^6\Sigma^+$ ($v = 1$) vibronic state exhibits more extensive local perturbations from the a $^4\Sigma^+$ ($v = 1$) vibronic state that affect even lower ($N = 1$) rotational levels.[14] In addition to the local perturbations, the A $^6\Sigma^+$ state exhibits homogeneous perturbations that contaminate the integrity of the $^6\Sigma^+$ state designation. *Ab initio* electronic structure calculations[16–19] predict that in addition to the a $^4\Sigma^+$ and A $^6\Sigma^+$ states, which correlate to the same dissociation limit of Cr(a^{5}S (3d^{5}4s^1)) + H(a ^{2}S), there are $^{4,6}\Delta$, $^{4,6}\Gamma$ and $^{4,6}\Sigma^+$ states that correlate in the dissociation limit to Cr(a^{5}D (3d^{4}4s^2)) + H(a^{2}S) with similar energy. The recently discovered B $^6\Pi$ state near the A $^6\Sigma^+$ ($v = 1$) vibronic state[14] is likely a member of this latter group.

To a first approximation, the magnetic tuning of a level can be predicted from the associated $^{2S+1}\Lambda$ term symbol and the eigenvalues and eigenvectors as derived from field-free parameters. Specifically, if it is assumed that X $^6\Sigma^+$ and A $^6\Sigma^+$ states are isolated Born–Oppenheimer states in the Hund's case (b) limit (*i.e.* the electron spin is not coupled to the

molecular axis) then upon application of a magnetic field each rotational level, N, splits into six ($= 2S + 1$) degenerate groups of $2N + 1$ levels. The tuning of each group is linear in magnetic field strength, B and is given by $g_S\mu_B B M_S$, where g_S is the electronic spin g-factor ($= 2.002$), μ_B is the Bohr magneton and M_S is the projection of the total electron spin on the quantization axis defined by the magnetic field. In reality the spin–rotation and spin–spin interactions in the X $^6\Sigma^+$ and A $^6\Sigma^+$ states of CrH are significant and the electron spin is not completely decoupled from the molecular axis even at high trapping fields (~ 2 T). Modeling the Zeeman effect is still, in principle, a straightforward process of accounting for the decoupling of the electron spin from the molecular frame and re-coupling to the laboratory frame. Unfortunately, the fact that the spin–rotation and spin–spin interactions in the X $^6\Sigma^+$ and A $^6\Sigma^+$ states are large indicates that the "goodness" of the Λ and Σ quantum numbers implied by the $^{2S+1}\Lambda$ term symbol is diminished from that of an isolated Born–Oppenheimer vibronic state. Born–Oppenheimer breakdown is particularly large for the eight nearly degenerate excited electronic states making an *a priori* prediction of the magnetic tuning of the A $^6\Sigma^+$–X $^6\Sigma^+$ spectral features impossible. Thus, an experimental measurement is required for determination of the optical Zeeman effect, the analysis of which gives insight into the nature of the multitude of interacting states.

The character of an electronic state may also be deduced from the analysis of the magnetic hyperfine interactions because these interactions depend upon the spatial distribution and spin density of the valence electrons at the proton. The determinable Fermi-contact, b_F and dipolar, c, parameters are related to the coordinates of the electron by:

$$b_F/\text{Hz} = \left(\frac{\mu_0}{4\pi h}\right)\left(\frac{8\pi}{3}\right)g_e g_N \mu_B \mu_N \frac{1}{S}$$
$$\times \langle \Lambda\Sigma = S | \sum_i \hat{s}_{zi}\delta_i(r)|\Lambda\Sigma = S\rangle_S \quad (1)$$

$$c/\text{Hz} = \left(\frac{\mu_0}{4\pi h}\right)\frac{3}{2}g_e g_N \mu_B \mu_N \frac{1}{S}$$
$$\times \langle \Lambda\Sigma = S | \sum_i \hat{s}_{iz}\frac{(3\cos^2-1)}{r_i^3}|\Lambda\Sigma = S\rangle_S \quad (2)$$

In eqns (1) and (2) Λ and Σ are the projection of total electronic orbital, **L**, and spin, **S**, angular momenta, respectively, on the internuclear axis. $\delta(r)$ is the Dirac delta function and r_i and θ_i are spherical polar coordinates of the electron relative to the proton. The proton b_F (-34.8 MHz) and c (42.3 MHz) parameters are small for the X $^6\Sigma^+$ state[10,11] because the unpaired electrons are primarily centered on the Cr nucleus. The negative value of b_F for the X $^6\Sigma^+$ state indicates that this term is dominated by spin-polarization of the Cr–H σ-bond and not direct spin density of the Cr-centered valence electrons at the proton. Changes to b_F and c upon excitation to the A $^6\Sigma^+$ state reflect subtle modifications to the electron distribution in the vicinity of the proton due to an alteration of the Cr-centered electrons.

2. Experimental

A cold sample of chromium monohydride was generated by laser ablating a solid chromium metal rod in a supersonic expansion similar to that of ref. 13 and 14, except that pure hydrogen gas instead of an argon/methane mixture was used as the reacting expanding gas. The typical conditions were 20 atm backing pressure, and 5 mJ of loosely focused 355 nm radiation from a Q-switched Nd:YAG laser. The supersonic free jet expansion was skimmed to produce a collimated molecular beam. The differentially pumped molecular beam chamber and optical Zeeman spectrometer are identical to those used previously in the optical Zeeman studies of CaH.[20] Approximately 30 mW of lightly focused power derived from a single longitudinal mode cw-Ti:sapphire laser was used to excite the (0, 0) and (1, 0) bands of the $A\,^6\Sigma^+$–$X\,^6\Sigma^+$ transition near 866 and 767 nm, respectively. The resulting laser induced fluorescence (LIF) was collected through a 870 ± 10 nm band pass filter and detected with a cooled GaAs photomultiplier tube. Photon counting techniques were used to process the signal.

Static homogeneous magnetic fields approaching 1100 Gauss were generated using a homemade electromagnet. This consisted of a pair of Helmholtz coils with ferromagnetic poles through which 12 mm holes were drilled to allow for the passage of the molecular beam.[20] The field was calibrated using a commercial Gauss meter. A polarization rotator and polarizing filter were used to orient the electric field vector of the linearly polarized laser radiation either parallel or perpendicular to the static magnetic field resulting in $\Delta M_J = 0$ or $\Delta M_J = \pm 1$ selection rules, respectively. The Zeeman-induced shifts and splittings were determined by simultaneously recording the transmission of the excitation laser through a temperature and pressure stabilized confocal etalon with a free spectral range of 753.58 MHz.[20]

3. Observations

The various spin fine structure components having identical parity and space fixed projection quantum numbers are mixed by the application of a magnetic field because the Zeeman Hamiltonian operator does not commute with the total angular momentum operator. Accordingly, the field-free spectra of numerous low-N branch features in the (0, 0) and (1, 0) bands of the $A\,^6\Sigma^+$–$X\,^6\Sigma^+$ transition were recorded and analyzed to obtain the field-free relative energies of the fine structure components. Ten and fourteen of the possible 18 branch features in the $A\,^6\Sigma^+$–$X\,^6\Sigma^+$ (0, 0) and $A\,^6\Sigma^+$–$X\,^6\Sigma^+$ (1, 0) band, respectively, that have either $N'' = 0$ or 1 were precisely measured field-free and are listed in Table 1. The branch labeling scheme is $^{\Delta N}\Delta J_{F_i}F_i''(N'')$ which is identical to that used in ref. 14. The "F_i" subscript takes on values of 1 to 6 for $J = N + S$ through $N–S$, respectively. Of the current set of spectral lines, only the $R_1(0)$, $R_1(1)$ and $R_2(1)$ features of the $A\,^6\Sigma^+$–$X\,^6\Sigma^+$ (0, 0) band had been measured previously in the Doppler-limited recording.[15] In the $A\,^6\Sigma^+$–$X\,^6\Sigma^+$ (1, 0) band all but the $^RQ_{32}(1)$ branch feature had been measured previously,[14] but at somewhat lower precision and resolution.

The observed and predicted spectra of the $^RQ_{21}(0)$ $A\,^6\Sigma^+$–$X\,^6\Sigma^+$ (0, 0) branch feature are presented in Fig. 1 along with the energy level pattern and quantum number assignment. The spectrum consists of two intense $\Delta F = \Delta J$ transitions and weaker $\Delta F \neq \Delta J$ features, where F is the total angular momentum. The field-free spectra were recorded from which proton magnetic hyperfine spitting in the $N = 0$ and 1 levels of the $A\,^6\Sigma^+$ ($v = 0$ and 1) vibronic states were obtained by combination/difference and using the known splittings for the $X\,^6\Sigma^+$ ($v = 0$) state.[11] The determined splittings and quantum number assignments are given in Table 2.

The $P_1(1)$, $^RP_{31}(0)$, $^RQ_{21}(0)$, and $R_1(0)$ lines of the $A\,^6\Sigma^+$–$X\,^6\Sigma^+$ (0, 0) band system and the $P_1(1)$, $^PQ_{12}(1)$, $^PR_{13}(1)$, $^RP_{31}(0)$, $^RQ_{21}(0)$ and $R_1(0)$ lines of the $A\,^6\Sigma^+$–$X\,^6\Sigma^+$ (1, 0) band system were selected for Zeeman measurements because these features probe all of the spin components (F_1, F_2 and F_3) of the $N = 0$ and 1 rotational levels in the $A\,^6\Sigma^+$ vibronic states. The $R_1(0)$ branch feature of the $A\,^6\Sigma^+$–$X\,^6\Sigma^+$ (1, 0) band is the most ideally suited for monitoring CrH in magnetic traps because it is associated with the lowest energy level, has the largest line strength factor and fluoresces off resonant at 874 nm. The off resonant fluorescent detection minimizes the background due to laser light scattering. Spectra of the $P_1(1)$ line in the $A\,^6\Sigma^+$–$X\,^6\Sigma^+$ (0, 0) and (1, 0) band systems observed field-free and in the presence of a magnetic field oriented parallel ($\Delta M_J = 0$) to the laser field are presented in Fig. 2. The assignments of the Zeeman spectral features of Fig. 2 are presented in Fig. 3 as are the energy levels as a function of magnetic field strength. The intense low wavenumber feature of the field-free spectra in Fig. 2 is the $F'' = 3 \rightarrow F' = 2$ transition and the intense high wavenumber feature is the $F'' = 4 \rightarrow F' = 3'$ transition. The weak, partially resolved, shoulder on the low wavenumber feature is the $F'' = 3 \rightarrow F' = 3$ transition. The hyperfine splitting is too small to discern in the energy level plots of Fig. 3. As is evident from Fig. 2 and 3, the Zeeman tuning of the $N = 0$, $J = 5/2$ (F_1) levels of $A\,^6\Sigma^+$ ($v = 0$) and $A\,^6\Sigma^+$ ($v = 1$) is significantly different. Also evident from Fig. 3 is that the electron spin in the $A\,^6\Sigma^+$ ($v = 0$), $A\,^6\Sigma^+$ ($v = 1$) and $X\,^6\Sigma^+$ ($v = 0$) states is still coupled to the molecular axis even at 4000 G and the approximately good quantum numbers are M_J and M_I, but not M_S. The uncoupling of the electron spin from the molecular axis results in a re-ordering into a pattern of six ($= 2M_S + 1$) distinct groups of levels[21] which is not evident in Fig. 3.

A total of 398 Zeeman shifted components were recorded at field strengths ranging from 424 to 1095 Gauss for the $A\,^6\Sigma^+$–$X\,^6\Sigma^+$ (0, 0) band system. The measured shifts, assignments and the differences between the observed and calculated shifts are collected in the tables of the ESI.† Similarly, at numerous field strengths ranging from 315 to 983 Gauss, the Zeeman shifted components corresponding to the spectral features in the $A\,^6\Sigma^+$–$X\,^6\Sigma^+$ (1, 0) band system were measured and are provided as ESI.† This data consisted of 362 features associated with the $N = 0$, $J = 5/2$ (F_1), 80 associated with the $N = 1$, $J = 3/2$ (F_3), 165 associated with the $N = 1$, $J = 5/2$ (F_2), and 216 associated with the $N = 1$, $J = 7/2$ (F_1), spin components of the $A\,^6\Sigma^+$ ($v = 1$) state.

This journal is © the Owner Societies 2007

Phys. Chem. Chem. Phys., 2007, **9**, 949–957 | 951

4. Analysis

Field- free energies

The Zeeman operator mixes the fine structure components. Therefore, accurately modeling the relative field-free energy spacing is a pre-requisite for the analysis of the Zeeman effect. The field-free energy levels of the A $^6\Sigma^+$ (v = 0 and 1) and X $^6\Sigma^+$ (v = 0) vibronic states were modeled using an effective Hamiltonian operator identical to that of ref. 10 and 11 which is reproduced here for convenience:

$$
\begin{aligned}
\boldsymbol{H}^{\mathrm{eff}}(^6\Sigma^+) = {} & B\boldsymbol{N}^2 - D\boldsymbol{N}^4 + \gamma \boldsymbol{N}\cdot\boldsymbol{S} + \frac{1}{2}\gamma_{\mathrm{D}}[\boldsymbol{N}\cdot\boldsymbol{S},\boldsymbol{N}^2]_+ \\
& + 10\gamma_{\mathrm{S}}T^3(\boldsymbol{L}^2,\boldsymbol{N})\cdot T^3(\boldsymbol{S},\boldsymbol{S},\boldsymbol{S})/[\sqrt{6}\langle\Lambda|\mathrm{T}_0^2(\boldsymbol{L}^2)\,|\Lambda\rangle] \\
& + \frac{2}{3}\lambda(3S_z^2 - \boldsymbol{S}^2) + \frac{1}{3}\lambda_{\mathrm{D}}[3S_z^2 - \boldsymbol{S}^2,\boldsymbol{N}^2]_+ + \frac{1}{12}\Theta[35S_z^4 \\
& - 30\boldsymbol{S}^2 S_z^2 + 25 S_z^2 - 6\boldsymbol{S}^2 + 3\boldsymbol{S}^4].b_{\mathrm{F}}\,(H)\,\boldsymbol{I}\cdot\boldsymbol{S} \\
& + c\,(H)\,(I_Z S_Z - \frac{1}{3}\boldsymbol{I}\cdot\boldsymbol{S}).
\end{aligned} \quad (3)
$$

Table 1 Field-free transition wavenumbers for the A $^6\Sigma^+$–X $^6\Sigma^+$ bands of CrH (in cm^{-1})

Assignment	F''	F'	(0,0) Observed[a]	Obs-calc	(1,0) Observed[b]	Obs-calc
$^PQ_{12}(1)$	2	2			18.6490	−0.0303
	3	2			18.6507	−0.0305
	2	3			18.6507	−0.0303
	3	3			18.6526	−0.0303
$P_1(1)$	3	2	38.6635	−0.0004	19.7840	−0.0265
	3	3	38.6649	−0.0005	19.7856	−0.0267
	4	3	38.6691	−0.0002	19.7897	−0.0264
$^PR_{13}(1)$	1	2			20.6322	−0.0243
	2	2			20.6358	−0.0245
	2	3			20.6379	−0.0241
$^RP_{31}(0)$	2	1	52.5663	−0.0347	33.6034	0.0789
	2	2	52.5677	−0.0346	33.6050	0.0788
	3	2	52.5712	−0.0347	33.6086	0.0788
$^RP_{53}(1)$	1	0	55.6380	0.0286	35.9234	−0.2664
	2	1	55.6425	0.0283	35.9278	−0.2670
$^RP_{42}(1)$	2	1			41.5052	0.1107
	3	2			41.5087	0.1106
$^RQ_{43}(1)$	1	1	62.8942	0.0088	43.4766	0.1049
	1	2			43.4782	0.1048
	2	1			43.4804	0.1049
	2	2	62.8996	0.0088	43.4820	0.1048
$R_1(0)$	2	3	63.4162	0.00283	44.3863	0.0513
	3	3	63.4201	0.00318	44.3899	0.0513
	3	4	63.4213	0.00317	44.3914	0.0513
$^RQ_{21}(0)$	2	2	67.7888	0.0256	49.73173	1.1784
	2	3	67.7910	0.0255	49.73483	1.1789
	3	2	67.7918	0.0251	49.73483	1.1779
	3	3	67.7948	0.0257	49.73783	1.1784
$^RP_{31}(1)$	2	2			52.1500	0.0099
	3	2			52.1521	0.0100
	2	3			52.1521	0.0096
	3	3			52.1542	0.0098
$R_3(1)$	1	2			54.1027	−0.0146
	2	2			54.1065	−0.0146
	2	3			54.1090	−0.0145
$^RQ_{32}(1)$	2	2	71.7568	−0.0414		
	3	3	71.7610	−0.0415		
$R_1(1)$	3	4	75.1370	0.0083	55.5957	0.0212
	4	4	75.1411	0.0086	55.5999	0.0215
	4	5	75.1421	0.0085	55.6014	0.0216
$R_2(1)$	2	3	76.1446	−0.0230	56.4570	−0.0432
	3	3	76.1467	−0.0228	56.4591	−0.0430
	3	4	76.1483	−0.0230	56.4611	−0.0429
$^RQ_{21}(1)$	3	3	77.3014	0.0025	57.5928	−0.0387
	3	4			57.5946	−0.0388
	4	3			57.5966	−0.0387
	4	4	77.3071	0.0026	57.5987	−0.0386
Std. dev. of fit:			0.0216 cm^{-1}		0.084 cm^{-1}	

[a] Observed transition wave number—11 500.0000 cm^{-1}. [b] Observed transition wave number—13 000.0000 cm^{-1}. [c] Strongly perturbed and not included in fit.
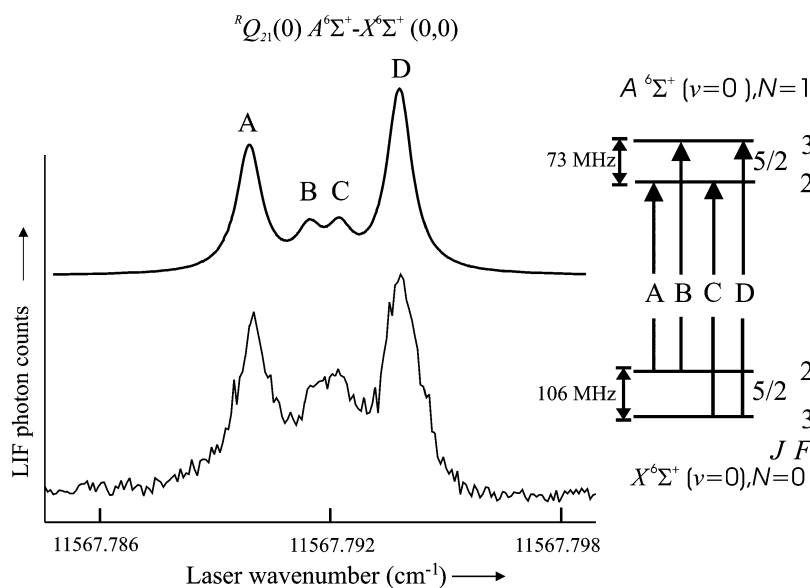
Fig. 1 The observed (lower) and predicted (upper) field-free spectra for the $^{R}Q_{21}(0)$ branch feature of the A $^{6}\Sigma^{+}$–X $^{6}\Sigma^{+}$ (0, 0) band along with the energy level pattern and quantum number assignment. The predicted spectrum has been shifted by -0.0255 cm^{-1}, to correct for a small local perturbation (see Table 1).

In eqn (3) γ and λ are the spin–rotation and spin–spin parameters, respectively and associate centrifugal distortion correction to these parameters are γ_{D} and λ_{D}. The parameter Θ multiplies the operator that accounts for the diagonal terms of the fourth-order spin–orbit interaction and the γ_{S} parameter multiplies the operator that accounts for third order spin–rotation. The high-order Θ and γ_{S} parameters are orders of magnitude smaller than γ and λ. The eigenvalues and vectors for the X $^{6}\Sigma^{+}$ (v = 0) and A $^{6}\Sigma^{+}$ (v = 0 and 1) states were obtained by a numerical diagonalization of a 12 × 12 matrix representation of the $\boldsymbol{H}^{\text{eff}}$, constructed using a Hund's case (a$_{\beta J}$), non-parity basis set, $\Psi = |n\Lambda;S\Sigma;J\Omega IFM_{F}\rangle$. The predicted pure rotational transition frequencies given in ref. 11 for the X $^{6}\Sigma^{+}$ (v = 0) state were reproduced using the previously published spectroscopic parameters[11] as a check of the procedure. Determination of an optimum set of field-free parameters for the A $^{6}\Sigma^{+}$ (v = 0 and 1) states was achieved in a two step procedure. First, the proton

hyperfine structure parameters (b_{F}(H) and c(H)) for the A $^{6}\Sigma^{+}$ (v = 0 and 1) states were obtained using the measured splittings given in Table 2 as input into a non-linear least squares fitting program. The magnetic hyperfine splittings are relatively insensitive to the fine structure parameters. Therefore, in this step the fine structure parameters (B, γ, γ_{S}, λ,) were constrained to the previously published[14,15] values. In the second step, these fine structure parameters and the origin, T_{v}, for the A $^{6}\Sigma^{+}$ (v = 0 and 1) states were optimized using a non-linear least squares fit of the measured optical transitions given in Table 1, excluding the strongly perturbed $^{R}Q_{21}(0)$ line of the (1, 0) band. In this fit all the ground state parameters were held fixed to those of ref. 11 and the excited state magnetic hyperfine parameters fixed to those derived in the first step. The data set was too restricted for the determination of γ_{S} and it was constrained to zero. The final set of optimized parameters and those previously obtained[14,15] are given in Table 3.

Table 2 The proton magnetic hyperfine splitting in the A $^{6}\Sigma^{+}$ state of CrH (in MHz)

| N | J | A $^{6}\Sigma^{+}$ (v = 0) | | A $^{6}\Sigma^{+}$ (v = 1) | |
		Obs.[a]	Obs-calc	Obs.	Obs-calc
0	5/2	40	−3	51	−4
1	3/2	42	4	45	−4
1	5/2	74	3	78	2
1	7/2	35	−1	47	−1
2	1/2	23	−6		
2	3/2	47	0	46	−4
2	5/2	66	−3	72	1
2	7/2	54	1	60	1
2	9/2	35	4	52	7
σ		4 MHz		5 MHz	
Parameters		b_{F} = 19(2) MHz		b_{F} = 22(2) MHz	
		c = 34(7) MHz		c = 28(8) MHz	

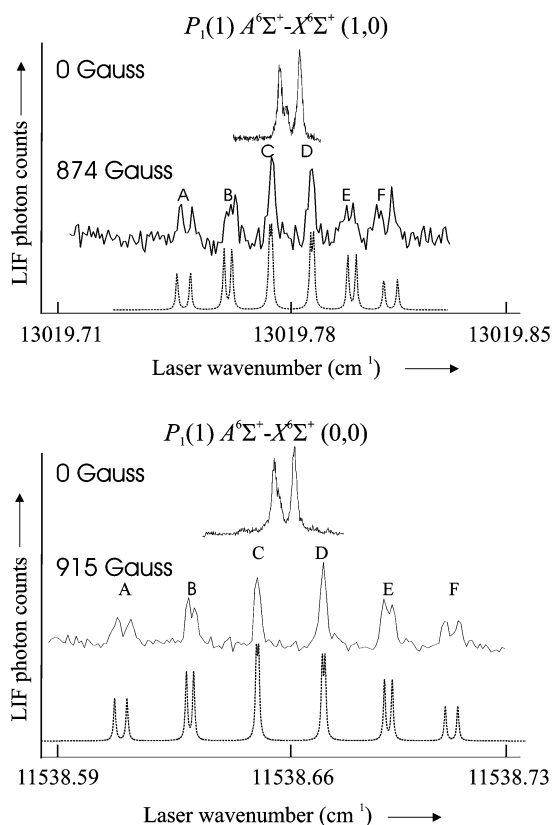[a] The upper energy level has total angular momentum $F = J + 1/2$.

The image shows scientific figures with spectra and energy level diagrams.

Fig. 2 The $P_1(1)$ line in the $A^6\Sigma^+$–$X^6\Sigma^+$ (1, 0) and (0, 0) band systems observed field free and in the presence of a magnetic field oriented parallel ($\Delta M_J = 0$) to the laser field. The dotted lines are predicted spectra generated using optimized field-free parameters and g_S-factors for the $A^6\Sigma^+$ state given in Tables 3 and 4. The spectroscopic parameters for the $X^6\Sigma^+$ ($v = 0$) state were constrained to those of ref. 4. The predicted spectrum of the $P_1(1)$ line in the $A^6\Sigma^+$–$X^6\Sigma^+$ (1, 0) branch has been shifted by 0.0267 cm^{-1}, to correct for a small local perturbation (see Table 1).

Fig. 3 The predicted energy levels as a function of magnetic field strength and the quantum number assignment of the spectral features presented in Fig. 2. The solid lines are levels of the $A^6\Sigma^+$ ($v = 0$) vibronic state and dotted lines are for levels of the $A^6\Sigma^+$ ($v = 1$) vibronic state. The field-free energies, $E(N = 0)$, of the $A^6\Sigma^+$ ($v = 0$) of the $A^6\Sigma^+$ ($v = 1$) vibronic states are 11552.64 and 13031.87 cm^{-1}, respectively. The magnetic tuning in the $A^6\Sigma^+$ ($v = 1$) state is considerably less than that of the $A^6\Sigma^+$ ($v = 0$) state because of mixing with the $a^4\Sigma^+$ state.

required for the analysis of the Zeeman effect and should not be used to extract other properties (*e.g.* bond distance) of the $A^6\Sigma^+$ ($v = 0$ and 1) states.

The Zeeman effect

The effective Hamiltonian operator for the Zeeman effect in the $A^6\Sigma^+$ ($v = 0$ and 1) and $X^6\Sigma^+$ ($v = 0$) vibronic states was taken as:[22,23]

$$H^{\mathbf{Zee}}(^6\Sigma) = g_s\mu_B\mathbf{S} \cdot \mathbf{B} + g_\ell\mu_B(S_xB_x + S_yB_y) - g_R\mathbf{N} \cdot \mathbf{B}. \quad (4)$$

In the effective Hamiltonian model, g_S is allowed to deviate from 2.002 to account for non-adiabatic contributions. The

As is evident from Table 1, all but the $N = 1$, $J = 5/2$ (F_2) energy level, which is the upper energy terminus of the $^RQ_{21}(0)$ branch feature, are fairly accurately predicted using the effective Hamiltonian approach. Except for, possibly, this energy level, the small discrepancies associated with using the derived effective parameters for the $A^6\Sigma^+$ ($v = 0$ and 1) states will not affect modeling the observed Zeeman effect. Note that the determined parameters only serve as a convenient method for modeling the field-free eigenvalues and eigenvectors as
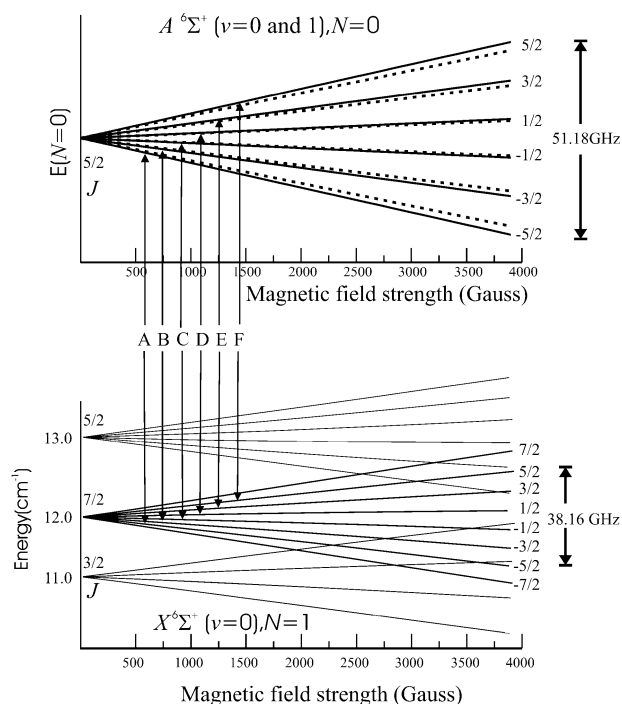
Table 3 Optimized spectroscopic parameters for the $A^6\Sigma^+$ state of CrH (in cm^{-1})

Parameter	$A^6\Sigma^+$ ($v = 0$)		$A^6\Sigma^+$ ($v = 1$)	
	Present[a]	Ref. 17	Present[b]	Ref. 16
T_v	11 552.635(13)	11 552.68416(75)	13 032.9233(99)	13 034.045(203)
B	5.2831(28)	5.272000(18)	5.1629(94)	5.1131(154)
γ	1.2974(19)	1.302067(70)	1.2931(66)	1.2870(315)
λ	1.5782(22)	1.57553(22)	1.5524(81)	1.5496(414)

[a] From a least squares fit of the transition wave numbers for the (0,0) band listed in Table 1. [b] From a least squares fit of the transition wave numbers for the (1,0) band listed in Table 1, excluding the $^RQ_{21}(0)$ line.

Table 4 Optimized magnetic g_S-factors for the A $^6\Sigma^+$ state of CrH

A $^6\Sigma^+$ ($v = 0$)		A $^6\Sigma^+$ ($v = 1$)		
$g_S{}^a$	σ(MHz)^b		$g_S{}^c$	σ(MHz)^b
2.0081(20)	40	$N = 0$, $J = 5/2$	1.7468(17)	38
		$N = 1$, $J = 3/2$	1.8760(30)	25
		$N = 1$, $J = 5/2$	1.7208(28)	31
		$N = 1$, $J = 7/2$	1.9123(25)	31

^{a} A simultaneous fit of the Zeeman shifts for the $P_1(1)$, $^RP_{31}$ (0), $^RQ_{21}(0)$ and $R_1(0)$ lines of the A $^6\Sigma^+$–X $^6\Sigma^+$(0,0) band. ^{b} Standard deviation of the fit. ^{c} Individual fits of the Zeeman shifts. The $P_1(1)$, $^PQ_{12}(1)$, $^PR_{13}(1)$ lines for the $N = 0$, $J = 5/2$ level; the $^RP_{31}(0)$ line for the $N = 1$, $J = 3/2$ level; the $^RQ_{21}(0)$ line for the $N = 1$, $J = 5/2$ level; the $R_1(0)$ line for the $N = 1$, $J = 7/2$ level.

other Zeeman parameters in eqn (4), are the anisotropic g-factor, g_ℓ and the rotational g-factor, g_R. The small magnetic contribution due to the proton nuclear spin has been ignored. Whereas there is no *a priori* method for estimating g_R, g_ℓ can often be adequately approximated for a state of Σ by the Curl relationship:[24]

$$g_l \approx -\gamma/2B, \qquad (5)$$

where B and γ are the rotation and spin–rotation parameters, respectively. The combined analysis of the mm-wave and LMR spectra[10,11] yielded values 2.001623(31), $-4.118(41) \times 10^{-3}$ and $-1.247(18) \times 10^{-3}$ for g_S, g_l and g_R, respectively, in the X $^6\Sigma^+$ ($v = 0$) vibronic state. The Curl relationship predicts a value for g_l of -4.10×10^{-3} and supports the use of this approximate relationship for CrH.

The matrix representation of $\hat{H}^{\mathbf{Zee}}$ is of infinite dimension and block diagonal in total angular momentum projection quantum number, M_F. The Zeeman effect in the $N = 0$ and 1 levels of the X $^6\Sigma^+$ ($v = 0$) and A $^6\Sigma^+$ ($v = 0$ and 1) vibronic states were accurately modeled by truncating the dimension of the representation to include only the $F = 0$, 1, 2, 3 and 4 field-free states which results in a 60×60 non-parity case ($a_{\beta J}$) matrix representation. The transition wavenumbers were calculated field free and in the presence of the magnetic field strength by taking the difference of appropriate eigenvalues obtained by numerical diagonalization of the 60×60 matrices for the X $^6\Sigma^+$ and A $^6\Sigma^+$ states. Zeeman shifts of the optical spectra were predicted and used as input into a non-linear least squares fitting procedure. In the end, the non-adiabatic parameters, g_ℓ, were held fixed to the values predicted by the Curl relationship: -0.1235 and -0.1238 for the A $^6\Sigma^+$ ($v = 0$) and A $^6\Sigma^+$ ($v = 1$) states, respectively. The rotational term, g_R, was constrained to zero. The final optimized set of g_S-factors for the A $^6\Sigma^+$ ($v = 0$ and 1) states is presented in Table 4.

The intensity. The quantum number assignment of the spectra was greatly assisted by modeling the intensities. The transition moments (TM) were calculated using:

$$\mathrm{TM} = [ev(\mathrm{X}\,^6\Sigma^+) \cdot |TMat| \, ev(\mathrm{A}\,^6\Sigma^+)] \qquad (6)$$

where *TMat* is the electric dipole operator transition moment matrix, $ev(\mathrm{X}\,^6\Sigma^+)$ and $ev(\mathrm{A}\,^6\Sigma^+)$ are the eigenvectors for the X $^6\Sigma^+$ and A $^6\Sigma^+$ states. In the predictions of the Zeeman spectra a 60×60 transition moment matrix was constructed

using the 60 Hund's case ($a_{\beta J}$) basis functions for $F = 0$, 1, 2, 3 and 4 levels. The transition moment matrix was of dimension 12 for modeling the field-free spectra. The transition moment was squared, multiplied by a Boltzmann factor commensurate with a rotational temperature of 10 K, and used in conjunction with a Lorentzian linewidth of 40 MHz full width at half maximum to predict each spectral feature. The predicted spectra were obtained by co-adding the individual spectral features. For spectra recorded at relatively high power, saturation effects were evident and the relative intensities of the weaker features were greater than predicted.

Discussion

A primary objective is to characterize the Zeeman tuning of the optical transitions that will be used for monitoring CrH in buffer-gas cooling and magnetostatic trapping experiments. The predicted intense $R_1(0)$ branch features of the A $^6\Sigma^+$–X $^6\Sigma^+$ (0, 0) and (1, 0) band systems are most ideally suited for monitoring CrH in magnetic traps. The predicted spectra of the $R_1(0)$ branch feature of the A $^6\Sigma^+$–X $^6\Sigma^+$ (1, 0) band systems over a range of magnetic field strengths from 0 to 0.8 T and with an orientation parallel ($\Delta M_J = 0$) to the laser field are presented in Fig. 4. The observed spectra recorded field free and in the presence of a 0.09 T field are also presented. The optimized parameters for the A $^6\Sigma^+$ state given in Tables 3 and 4 and the ground state parameter of ref. 11 were used for these predictions. Upon the application of only a modest magnetic field, the $R_1(0)$ spectrum splits into six ($= 2J'' + 1$) sets of closely spaced doublets because the proton nuclear spin is easily de-coupled from the molecular axis and hence M_J and M_I become the approximately good quantum numbers. The tuning of the six components, labeled "A" through "F" in Fig. 4, over the 0.1 to 0.8 T range, are plotted on the right hand side of Fig. 4. They exhibit significant non-linearity because the electron spin, S, is decoupling from the molecular axis at different rates in the $N = 1$, $J = 7/2$ (F_1) level of the A $^6\Sigma^+$ ($v = 1$) state and the $N = 0$, $J = 5/2$ (F_1) level of the X $^6\Sigma^+$ states upon application of the magnetic field. The predicted tuning of each of the six spectral features of the $R_1(0)$ branch feature of the A $^6\Sigma^+$–X $^6\Sigma^+$ (0, 0) and (1, 0) band systems were fit to a second-order polynomial, the results of which are presented in Table 5. These parameters should reliably predict the magnetic tuning over the fields that are typically used in a magnetic trap.

The Zeeman tuning of all the probed levels in the A $^6\Sigma^+$ ($v = 1$) state is slower than that expected for a state of pure $^6\Sigma^+$ character and accordingly the determined effective g_S-factors are less than 2.002. The largest deviation of the determined g_S-factor from the expected value of 2.002 is for the $N = 1$, $J = 5/2$ (F_2) level of the A $^6\Sigma^+$ ($v = 1$) state which is the level that also exhibits the strongest field-free energy perturbation (see Table 1 and ref. 16) suggesting that mixing with the a $^4\Sigma^+$ state is responsible for the slower than expected tuning. The determined relative magnitudes of the deviations from 2.002 for the four levels of the A $^6\Sigma^+$ ($v = 1$) state probed can be used to identify the nature of the perturbing states. The appropriate perturbation selection rules for the change in angular momentum is $\Delta J = 0$, because the magnetic
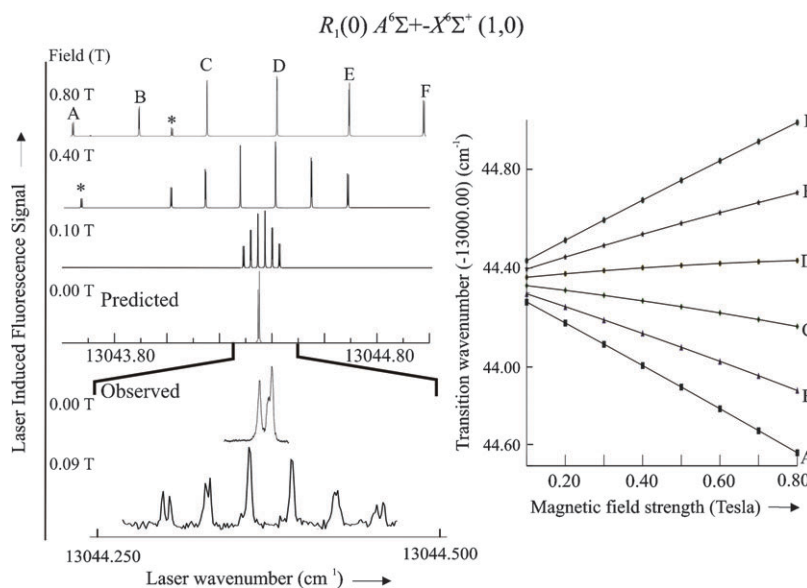
This journal is © the Owner Societies 2007

Phys. Chem. Chem. Phys., 2007, **9**, 949–957 | 955

Fig. 4 The observed and predicted $R_1(0)$ line of the A $^6\Sigma^+$–X $^6\Sigma^+$ (1, 0) band system for parallel polarization as a function magnetic field strength (left panel). On the right hand side is a plot of the tuning character of spectral feature "A" through "F" over the range 0.1 T to 0.8 T. The solid lines are the tuning curves predicted from the second order polynomial fit of the predicted shifts. The fitted polynomial parameters are presented in Table 5. The quantum number assignment for "A" through "F" are $M_J = -5/2$ through $+5/2$, respectively. The feature marked with an asterisk is a component of the $^RQ_{43}(1)$ line.

hyperfine interaction is very small. The selection rule for parity is $\pm \leftrightarrow \pm$. For the case of a $^6\Sigma^+ \sim {}^4\Sigma^+$ interaction, the additional selection rules are $\Delta N = 0$, 2 and 4.[15] Thus the $N = 1$, $J = 5/2$ (F_2) level of the nominal A $^6\Sigma^+$ ($v = 1$) state can interact with the $N = 1$, $J = 5/2$ (F_1) and $N = 3$, $J = 5/2$ (F_3) levels of the nominal a $^4\Sigma^+$ state. Evidently the $N = 1$, $J = 5/2$ (F_1) and $N = 3$, $J = 5/2$ (F_3) levels of the nominal a $^4\Sigma^+$ state tune more slowly than those of the $N = 1$, $J = 5/2$ (F_2) level of the nominal A $^6\Sigma^+$ ($v = 1$) state. The tuning of these three levels will be given approximately by the expectation value of $\hat{H}^{Zee}$ in a Hund's *case b* wavefunction. Using the expression for the matrix elements of ref. 23 this expectation value is:

$$\langle Case\ b|H^{Zee}(^6\Sigma)|Case\ b\rangle = g_J\mu_B B_z M_J$$
$$= g_S \frac{[S(S+1) + J(J+1) - N(N+1)]}{2J(J+1)}\mu_B B_z M_J. \qquad (7)$$

Effective g_J-factors predicted by eqn (7) for the $N = 1$, $J = 5/2$ (F_2) level of a $^6\Sigma^+$ state and the $N = 1$, $J = 5/2$ (F_1) and $N = 3$, $J = 5/2$ (F_3) levels of a $^4\Sigma^+$ state are 1.7735, 1.2014

and 0.0572, respectively. Both of the levels of the Hund's *case b* $^4\Sigma^+$ state tune more slowly than the $N = 1$, $J = 5/2$ (F_2) level of the Hund's *case b* $^6\Sigma^+$ state. If it is assumed that as in the case of the A $^6\Sigma^+$ ($v = 0$) state[15] the $\Delta N = 2$ interaction dominates, then the sole perturbing level (*i.e.* the $N = 3$, $J = 5/2$ (F_3) level of the a $^4\Sigma^+$ state) tunes approximately 31 times slower than the $N = 1$, $J = 5/2$ (F_2) level of the nominal A $^6\Sigma^+$ ($v = 1$) state. The ratio of the observed to expected g_S-factor ($= 1.721/2.002 = 0.860$) and the Hund's *case b* tuning rate for a $N = 3$, $J = 5/2$ (F_3) level of a $^4\Sigma^+$ state and a $N = 1$, $J = 5/2$ (F_2) level of a $^6\Sigma^+$ state predicts that $N = 1$, $J = 5/2$ (F_2) level of the A $^6\Sigma^+$ ($v = 1$) state is an admixture of approximately 14.5% ($= 100\% \times (1 - 0.860) \times 31/30$) of the $N = 3$, $J = 5/2$ (F_3) level of the a $^4\Sigma^+$ state. The $N = 1$, $J = 7/2$ (F_1) level of the A $^6\Sigma^+$ ($v = 1$) state interacts with the $N = 3$, $J = 7/2$ (F_2) level of the a $^4\Sigma^+$ state, which in the Hund's *case b* limit has a g_J-factor of 0.4767. Thus it is expected that the effective g_S-factor for the $N = 1$, $J = 7/2$ (F_1) level of the A $^6\Sigma^+$ ($v = 1$) state will be larger than that of the $N = 1$, $J = 5/2$ (F_2) level of the A $^6\Sigma^+$ ($v = 1$) state, in agreement with the observation.

Table 5 Second-order polynomial fit of the magnetic tuning of the $R_1(0)$ line

Feature[a]	A $^6\Sigma^+$–X $^6\Sigma^+$ (0,0)			A $^6\Sigma^+$–X $^6\Sigma^+$ (1,0)		
	a[b]/cm^{-1}	b/cm^{-1} T^{-1}	c/cm^{-1} T^{-2}	a/cm^{-1}	b/cm^{-1} T^{-1}	c/cm^{-1}/T^{-2}
A	11 563.4134	−0.7577	−0.03756	13 044.3470	−0.8386	−0.03610
B	11 563.4138	−0.4581	−0.06149	13 044.3470	−0.5032	−0.06158
C	11 563.4132	−0.1535	−0.07226	13 044.3470	−0.1682	−0.07595
D	11 563.4138	0.1488	−0.08101	13 044.3471	0.1665	−0.07720
E	11 563.4132	0.4554	−0.07411	13 044.3468	0.5035	−0.06878
F	11 563.4134	0.7571	−0.04577	13 044.3466	0.8406	−0.04586

[a] The six spectral features of Fig. 4 or the equivalent for the (0,0) band. [b] Transition wavenumber (cm^{-1}) = $a + b \times B + c \times B^2$ with B = magnetic field strength in Tesla.

As expected, the proton magnetic hyperfine parameters are two orders of magnitude smaller than that of the H-atom because the unpaired electrons remain metal centered in both the $A\,^6\Sigma^+$ and $X\,^6\Sigma^+$ states. The magnetic hyperfine interaction in the $A\,^6\Sigma^+$ ($v = 1$) state does not exhibit the same strong rotational dependence as the Zeeman effect. This suggests that the $A\,^6\Sigma^+$ and perturbing a $^4\Sigma^+$ state arise from similar molecular orbital configurations. A simple picture for bonding in the low-lying group of excited states[17] is that the Cr atom in the $a\,^5D$ ($3d^44s^2$) state approaches the ground state hydrogen atom and a 4s/4p hybrid orbital is formed. The hybrid orbit directed towards the H-atom forms a σ-type bond, whereas the hybrid orbit pointed away from the bond remains singly occupied. In the $A\,^6\Sigma^+$ state the electron in this back-polarized 4s/4p hybrid orbital is high-spin coupled to four high-spin coupled unpaired electrons in the 3d orbitals. In the a $^4\Sigma^+$ state the electron in this back-polarized 4s/4p hybrid orbital is low-spin coupled. The nature of the electron in this back-polarized 4s/4p hybrid orbital has a negligible effect on the electron density in the spatially removed region of the proton and thus the hyperfine interaction in the $A\,^6\Sigma^+$ and a $^4\Sigma^+$ state, or any admixture thereof, will be similar. The Fermi contact parameter, b_F, for the $A\,^6\Sigma^+$ state is determined to be positive whereas it is negative for the $X\,^6\Sigma^+$ state.[11] Evidently in the $X\,^6\Sigma^+$ state, the direct contribution to the spin density at the proton is larger than the spin-polarization effects which contribute with opposite sign.[22,25] Upon excitation to the $A\,^6\Sigma^+$ state a portion of the metal centered spin density is shifted away from the Cr–H bond *via* the occupation of the back-polarized 4s/4p hybrid orbital. This reduces the spin-polarization of the electrons in the σ-type bond resulting in the domination of the direct spin density contribution. Similar change in sign of b_F has been observed in excitation from the $X\,^7\Sigma^+$ state to the a $^7\Pi$ state of MnH.[26]

Conclusion

A pulsed molecular beam of cold ^{52}CrH has been generated by laser ablation techniques and detected by near natural line width limited laser induced fluorescence spectroscopy. The magnetic tuning of the low-N lines of the $A\,^6\Sigma^+$–$X\,^6\Sigma^+$ (0, 0) and (1, 0) bands have been experimentally characterized and modeled using an effective Hamiltonian. The magnetic g-factors for the $A\,^6\Sigma^+$ ($v = 1$) state deviate significantly from those expected for an isolated state $^6\Sigma^+$ state. Interaction with the nearly degenerate a $^4\Sigma^+$ provides a qualitative explanation of the deviation of the g-factors and the observed proton magnetic hyperfine interactions. Further insight into the nature of the interacting $A\,^6\Sigma^+$ and a $^4\Sigma^+$ states will be obtained from optical Stark measurements, which are currently being pursued in our laboratory. The experimentally determined magnetic tuning characteristics of the $R_1(0)$ branch feature of the $A\,^6\Sigma^+$–$X\,^6\Sigma^+$ (1, 0) band system will be used for *in situ* monitoring of buffer gas cooling and magnetic trapping of CrH.

References

1 J.-P. Uzan, *Rev. Mod. Phys.*, 2003, **75**, 403–455.
2 J. J. Hudson, B. E. Sauer, M. R. Tarbutt and E. A. Hinds, *Phys. Rev. Lett.*, 2002, **89**, 023003.
3 D. DeMille, *Phys. Rev. Lett.*, 2002, **88**, 067901.
4 H. L. Bethlem and G. Meijer, *Int. Rev. Phys. Chem.*, 2003, **22**, 73, and references therein.
5 J. D. Weinstein, R. deCarvalho, T. Guillet, B. Friedrich and J. M. Doyle, *Nature*, 1998, **395**, 148.
6 R. V. Krems, A. Dalgarno, N. Balakrishnan and G. C. Groenenboom, *Phys. Rev. A*, 2003, **67**, 060703.
7 H. Cybulski, R. V. Krems, H. R. Sadeghpour, A. Dalgarno, J. Klos, G. C. Groenenboom, A. van der Avoird, D. Zgid and G. Chalasinski, *J. Chem. Phys.*, 2005, **122**, 094307.
8 K. Maussang, D. Egorov, J. S. Helton, S. V. Nguyen and J. M. Doyle, *Phys. Rev. Lett.*, 2005, **94**, 123002.
9 J. M. Bakker, M. Stoll, D. R. Weise, O. Vogelsang, G. Meijer and A. Peters, *J. Phys. B: At. Mol. Opt. Phys.*, 2006, **39**, S1111.
10 S. M. Corkery, J. M. Brown, S. P. Beaton and K. M. Evenson, *J. Mol. Spectrosc.*, 1991, **149**, 257.
11 J. J. Harrison, J. M. Brown, D. T. Halfen and L. M. Ziurys, *Astrophys. J.*, 2006, **637**, 1143.
12 A. Burrows, R. S. Ram, P. Bernath, C. M. Sharp and J. A. Milsom, *Astrophys. J.*, 2002, **577**, 986.
13 S. Shin, D. J. Brugh and M. D. Morse, *Astrophys. J.*, 2005, **619**, 407.
14 P. K. Chowdhury, A. J. Merer, S. J. Rixon, P. F. Bernath and R. S. Ram, *Phys. Chem. Chem. Phys.*, 2006, **8**, 822.
15 R. S. Ram, C. N. Jarman and P. F. Bernath, *J. Mol. Spectrosc.*, 1993, **161**, 445.
16 D. Dai and K. Balasubramanian, *J. Mol. Spectrosc.*, 1993, **161**, 455.
17 C. W. Bauschlicher, Jr, R. S. Ram, P. F. Bernath, C. G. Parsons and D. Galehouse, *J. Chem. Phys.*, 2001, **115**, 1312.
18 G. Ghigo, B. Roos, P. C. Stancil and P. F. Weck, *J. Chem. Phys.*, 2004, **121**, 8194.
19 S. Koseki, T. Matsushita and M. Gordon, *J. Phys. Chem. A*, 2006, **110**, 2560.
20 J. Chen, J. Gengler, T. C. Steimle and J. M. Brown, *Phys. Rev. A*, 2006, **73**, 012502.
21 G. Berden, R. Engeln, P. C. M. Christiansen, J. C. Maan and G. Meijer, *Phys. Rev. A*, 1998, **58**, 3114.
22 W. Weltner, Jr, *Magnetic Atoms and Molecules*, Dover Publications Inc., New York, 1983.
23 J. M. Brown and A. Carrington, *Rotational Spectroscopy of Diatomic Molecules*, Cambridge University Press, Cambridge, 2003.
24 R. F. Curl, *Mol. Phys.*, 1965, **9**, 585.
25 M. L. Munzarova, P. Kubacek and M. Kaupp, *J. Am. Chem. Soc.*, 2000, **122**, 11900–11913.
26 T. D. Varberg, J. A. Gray, R. W. Field and A. J. Merer, *J. Mol. Spectrosc.*, 1992, **156**, 296–318.

This journal is © the Owner Societies 2007

Phys. Chem. Chem. Phys., 2007, **9**, 949–957 | 957